Three-Dimensional Microscale Simulation of Colloidal Particle Transport and Deposition in Chemically Heterogeneous Capillary Tubes

Yajie Li[1,2], Azita Ahmadi[2*], Aziz Omari[3], Hongting Pu[4]

1 : School of Materials Science and Engineering, Shanghai University, Shanghai, 200444, China

2 : I2M, Arts et Métiers Paris-Tech, CNRS, Esplanade des Arts et Métiers, 33405 Talence Cedex, France

3 : I2M, Bordeaux-INP,CNRS, Esplanade des Arts et Métiers, 33405 Talence Cedex, France

4 : School of Materials Science and Engineering, Tongji University, Shanghai, 201804, China

Corresponding authors :

* Azita Ahmadi

Mailing address: I2M-TREFLE, UMR CNRS, Arts et Métiers Paris-Tech, Esplanade des Arts et Métiers, 33405 Talence Cedex, France

E-mail: azita.ahmadi-senichault@u-bordeaux.fr

Phone: + 33 0556846394

Abstract: The effect of surface chemical heterogeneity and hydrodynamics on particle transport and deposition in porous media was investigated by microscale simulations using a colloidal particle tracking model, called 3D-PTPO (Three-dimensional particle tracking model by Python® and OpenFOAM®) code. This work is aimed as a step toward modeling of transport and deposition in porous media idealized as a bundle of straight capillary tubes. Therefore, our focus is put upon a three-dimensional capillary with periodically repeating chemically heterogeneous surfaces namely crosswise strips patterned and chess board patterned. The main feature of this recent model is to renew the flow field by reconstructing the pore structure, to take the pore surface modification induced by the volume of the deposited particles into account. The dependency of the deposition probability and the dimensionless surface coverage (Γ/Γ_{RSA}) on the frequency of the pitches (λ), the Péclet number (Pe) and the favorable area fraction (θ), as well as the distribution of the spatial density of deposited particles along the capillary tube were studied. The results indicate that particles tend to deposit at the leading and trailing edges of the favorable strips, and the deposition is more uniform along the patterned capillary compared to the homogeneous one. In addition, for the chemically heterogeneous capillary, in a similar manner as for the homogeneous one, a definite plateau exists for the Γ/Γ_{RSA} at low Péclet values. For high Pe values, the declining trend for Γ/Γ_{RSA} versus Pe is in good agreement with the derived power law dependence already observed in the literature for fully adsorbing surfaces. Moreover, for fixed θ the deposition probability is linearly correlated with λ and for given λ, such a deposition probability is also a linear function of θ.

Keywords: Microscale simulation; Capillary tube; Particle deposition; Chemical heterogeneity; Crosswise strips pattern; Chess board pattern.

1. Introduction

Colloidal particle transport and deposition (irreversible adsorption) processes in porous media are of great environmental and industrial interest since they are critical to numerous applications ranging from drug delivery to drinking water treatment [1-5]. Accordingly, particle deposition on homogeneous porous media has been extensively studied both experimentally and a rich literature thereupon is available [6-11] and theoretically [12-16].

To model such a particles transport, the first approach was to consider spatial and temporal variations of colloid concentration C incoming at a concentration C_0 in a representative elementary volume (REV). This black box Eulerian formulation results in a convection-diffusion partial differential equation that contains terms that account for short range hydrodynamic and physicochemical interaction forces between particles and the porous medium skeleton. Usually hydrodynamic interactions are introduced through the hydrodynamic correction factors and non-hydrodynamic interactions are introduced through a DLVO potential that encompasses at least Van der Walls and electrostatic interactions. When solved for the outgoing concentration in a 1D situation, it mimics common column experiments. This allows interpretation of experimental breakthrough curves and evaluation of the pertinence of modeling refinements.

At the pore scale level usually starting from the Happel cell model, the focus is put on the determination of collector efficiency or the Sherwood number and on how they depend on hydrodynamic and physico-chemical conditions. Moreover, in most of considered systems, colloids and substrate are chemically homogeneous with smooth surfaces and the reader may refer to the review proposed by Molnar et al. for an up-to-date analysis [17].

It is however well known that natural porous media are by nature of non-uniform chemical composition at the nanoscale or even at the microscale with only a fraction of their surface favorable for colloid deposition. Such heterogeneities consist in general in chemical patches that are actually randomly distributed over the medium and whose macroscopic impact depends mainly on the fraction of the adsorbing surface and the particle to patch size ratio. When the patch dimensions are much larger than the particle size, the spatial averaging in patch models gives accurate results in accordance with colloid transport experiments [18]. Typical experiments are performed on columns packed with chemically heterogeneous sand grains at various degrees of patch-wise charge heterogeneity and several spatial distributions of heterogeneity. Indeed in this case the colloid deposition rate was found to be directly proportional to the degree of porous medium chemical heterogeneity and largely insensitive to the spatial distribution of patch-wise chemical heterogeneity [19]. However, when the patch size is comparable to that of the particle, both the fraction of adsorbing surface and the particle to patch size ratio become relevant parameters.

Under diffusion-controlled conditions, Adamczyk and co-workers have studied the deposition of colloid particles on heterogeneous surfaces by means of numerical simulations of the Monte Carlo type. They considered adsorption sites as having the shape of circular disks with a finite size comparable with the size of adsorbing spheres [20]. They showed that on one hand when the particle/site size ratio is increased both adsorption kinetics and the maximum surface coverage increased for a fixed site density and as long as the particle/site size ratio is greater than 10, the available Random Sequential Adsorption theory extended to Random Site Surface RSA-RSS still works. This was experimentally confirmed through investigation of latex particles deposition on heterogeneous surfaces [21]. However when adsorption sites are attractive spheres that are deposited in advance on a flat surface, the problem is more complicated since it is of 3D nature [22]. However and as in natural substrates the charge heterogeneity is random and of arbitrary shape, systematic evaluation of deposition characteristics on such substrates is not straightforward thus heterogeneous surfaces are considered as patterned and are usually modeled by alternating adsorbing and non-adsorbing strips of given widths and densities.

To simulate colloid surface deposition one can adopt a Lagrangian or an Eulerian approach. As usual in the Lagrangian approach, individual particles are followed until they adsorb on the pore wall by solving the Langevin equation with the incorporation of retardation functions to account for hydrodynamic and non-hydrodynamic particle/collector interactions through a DLVO potential [23-28].When this approach is applied to porous media represented as a packed bed of spherical collectors, calculations become difficult to tract if reasonable porosity is targeted [29]. As we will see below, in this paper the accent is put upon taking into account the effect of the already adsorbed particles on flow and therefore further deposition rendering the incorporation of short range interactions still less tractable.

The most used simulation method is the Eulerian one which consists in solving a diffusion-convection-migration partial differential equation where colloid/collector hydrodynamic coupling is obtained by introducing the hydrodynamic correction factors while non-hydrodynamic

colloid/collector interaction is locally calculated knowing the nature of surfaces facing each other [30]. This approach was used for modelling colloid deposition on janus spherical collectors [31], impinging jet flow of dilute suspension on a flat heterogeneous surface [32] and colloid deposition in patterned cylindrical microchannels [33]. All these works demonstrate that deposition concentration profile closely mimics the spatial distribution of the heterogeneity. Moreover, for strip-patterned heterogeneity, a sharp deposit concentration peak is observed at the leading edge of each favorable strip before it decays rapidly and attains a plateau over the rest of the strip but it still remains above the concentration profile for a homogeneous surface. In case of a micro-patterned channel, colloids deposition is predicted to be more regular along the channel than in the homogeneous case where particles will mainly deposit within a short distance from the inlet. From the concentration profile, the local and average Sherwood number (or collector efficiency) may be calculated. It is then demonstrated that the relative favorable surface is not the only relevant parameter but the spatial distribution of favorable patches is also important. Hence for a given fraction of favorable surface area, a larger number of favorable patches results in better deposition efficiency.

In all these models, the perfect skin condition was always considered and consequently they ignore any modification of flow pattern that would result from finite size particle deposition. This is however believed to play an important role in the strength of hydrodynamic shadowing effect especially when particle size to pore size ratio is not negligible and well after the beginning of deposition when surface coverage becomes significant. This was shown to be relevant for colloid deposition on homogenous surfaces of pores of various shapes. In constricted geometries, deposition was shown to occur mainly in pore bodies rather than in pore throats where the hydrodynamic shadowing effect was more efficient [34, 35]. In case of geochemically heterogeneous porous media, this is expected to have even more impact on deposit structure with a determinant influence of the ratio of colloid size to characteristic size of heterogeneity besides the pore geometry and the flow rate. Therefore, the aim of the present paper is to take into account the finite size of adsorbed particles when investigating colloids deposition in three-dimensional axisymmetric pores whose surface consists in a periodic repetition of adsorbing and non-adsorbing surfaces with a specified topology. Here, we focus on the dependence of deposition probability and the surface coverage on parameters such as the fraction of surface heterogeneity, the spatial distribution and topology of the heterogeneous surface elements as well as the flow strength. For that purpose, we use a home-made Lagrangian code that is basically a three-dimensional particle tracking model using Python® and OpenFOAM® which is presented in the next part. In the third part, simulation results are presented and discussed in the light of up to date published literature dealing with colloids deposition on heterogeneous surfaces and particularly emphasizing the effect of flow change induced by adsorbed particles on the structure of the deposit. The paper ends with some concluding remarks.

2. Simulation cases, tools and procedure

The present work is restricted to the modeling of the process of transport and deposition of positively charged particles in a chemically heterogeneous capillary, as an element of many idealized porous medium models such as bundle of capillaries or more complex pore network models. Equivalently, we consider a single cylindrical capillary with periodically repeating heterogeneity under the form of patterned or square patch-wise adsorbing surfaces (see Figure 1). In case of transverse strips, the leading one is always positively charged and therefore non-adsorbing. The frequency of the pitches (λ) is calculated as the ratio of the length of the capillary L to the total width

p of a pitch; p being the sum of widths of adsorbing element w_a and non-adsorbing one w_{na}. The fraction of favorable area is $\theta = A_f/A_t$, with A_f the area of the surface wall favorable for particles deposition and A_t the total surface of the capillary wall. Here we take L = 15 µm and a capillary radius R = 4 µm and the considered colloids are spherical with a radius, a_p = 0.2 µm giving a ratio R/a_p=20 that is not high enough to neglect the change of the flow structure due to particles deposition but it is sufficient to consider a particle approaching a flat solid surface. A sensitivity analysis was undertaken beforehand to explore the effect of mesh numbers on the accuracy of our results by varying the number of grid blocks used for the numerical simulations. The deposition probability and distribution of deposited particles are compared for various mesh numbers going from 30,000 to 960,000. The results indicate that 120,000 grid blocks (40 x 40 x 75) are sufficient for our computations.

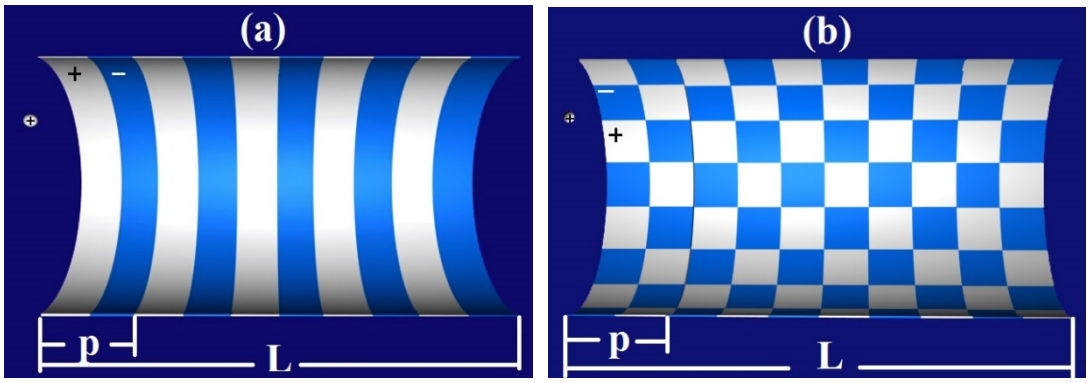

Figure 1 : Surface heterogeneity is modeled as alternate attractive and repulsive bands: (a): Crosswise strips patterned; (b): Chess board patterned. White and blue colors represent positively and negatively charged regions respectively. Particles are positively charged.

2.1 General hypothesis

In the present work the following assumptions are adopted [36, 37]:

(1) The fluid is Newtonian and incompressible.

(2) The particle Reynolds number defined as $\mathrm{Re} = \rho \bar{u} a_p / \mu$ (where ρ and µ are the fluid density and dynamic viscosity and $\bar{u}$ is the fluid's mean velocity under clean bed conditions) is so small that the flow may be considered as laminar and non-inertial.

(3) Deposition is irreversible and both hydrodynamic and physico-chemical removal of deposited particles are prohibited.

(4) The scale of the variation of the flow velocity over a_p is small compared to the maximum velocity. We can reasonably assume that the particle transported by the flow is a mass point.

(5) The non-hydrodynamic particle-particle interaction is purely repulsive; therefore particles deposit is a monolayer.

2.2 Governing equations and boundary conditions

The governing equations for the creeping flow of an incompressible Newtonian fluid are the Stokes equations given by [38] :

$$0 = -\nabla p + \mu \nabla^2 \mathbf{v} \qquad (1)$$

$$\nabla \cdot \mathbf{v} = 0 \qquad (2)$$

where p is the pressure and **v** stands for the fluid velocity.

A no-slip boundary condition is applied on the pore wall and on the interface between the fluid and deposited particles. At the inlet, the pressure is set to a predefined value, while at the outlet it is set to zero. In order to fulfill the requirement of creeping flow and to investigate a large range of Péclet numbers, the pressure at the inlet will be varied between 10^{-5} and 10 Pa. The Péclet number is defined as:

$$Pe = \frac{\bar{u}\, a_p}{D} \tag{3}$$

where D is the bulk diffusion coefficient of the particles in the fluid, $\bar{u}$ is the average value of velocity along the tube axis.

2.3 Methodology and tools

Since the incoming suspension is considered to be dilute, particles are injected individually, randomly and sequentially at the inlet of the geometry [5]. A Lagrangian method is then used to track the trajectories of the colloidal particles and once the injected particle is deposited onto the capillary wall or leaves the domain, another particle is injected. This process is then repeated until the pre-defined cut-off value of deposition probability (2%) is reached. The deposition probability is defined as the ratio of the number of deposited particles over the number of injected particles. Simulations are carried out using the 3D-PTPO code that combine OpenFOAM® (Open Field Operation and Manipulation) and Python® softwares. The detailed steps of the 3D-PTPO code are as follows: firstly, the flow field is computed using OpenFOAM® software by solving the equation of motion and obtained flow field data are recorded. Then a particle, that is reduced to its center of mass, is injected at the entrance plane (z = 0) with the initial coordinates (x,y) generated by two independent pseudo-random series [39]. Secondly, the injected particle is tracked using a code developed in Python®. To track the movement of the particle in the flow domain the particle velocity vector $\mathbf{V}$ at every position within the domain is calculated by summing its advection velocity $\mathbf{V_{adv}}$ and the Brownian diffusion velocity $\mathbf{V_{diff}}$. $\mathbf{V_{adv}}$ is obtained from the recorded flow field by interpolating the velocity of the nearest eight mesh-nodes surrounding the actual particle position. $\mathbf{V_{diff}}$ represents the random velocity of the particle due to Brownian motion at every time-step and is calculated as:

$$\mathbf{V}_{\mathbf{diff}} = \left\|\mathbf{V}_{\mathbf{diff}}\right\|\left(\alpha\mathbf{i}+\beta\mathbf{j}+\gamma\mathbf{k}\right)$$
$$\alpha=\frac{a}{\sqrt{a^2+b^2+c^2}}\ ;\ \beta=\frac{b}{\sqrt{a^2+b^2+c^2}}\ ;\ \gamma=\frac{c}{\sqrt{a^2+b^2+c^2}} \tag{4}$$
$$\left\|\mathbf{V}_{\mathbf{diff}}\right\|=\sqrt{\frac{D}{t_r}}=\sqrt{\frac{kT}{6\pi\mu a_p t_r}}$$

where a, b and c are random numbers drawn from a uniform distribution between -1 and 1; α, β and γ are determined by the normalization of the three random numbers, thus giving a unit vector with a random direction $\alpha\mathbf{i}+\beta\mathbf{j}+\gamma\mathbf{k}$, k is the Boltzmann constant and T is the absolute temperature. The values of the parameters used in the simulation are summarized in Table 1. Here we neglect the particle mobility reduction near the wall that alters its diffusivity tensor. Indeed, the explicit evaluation of this reduction is of no means in this work since we do not calculate hydrodynamic forces acting on a physical particle moving near the wall albeit one could have advocated a

phenomenological correction of the diffusivity coefficient as particles approach the wall. The reference time t_r that appears in Eq. 4 is chosen as [37]:

$$t_r=\zeta/(2\ u_{max}) \quad (5)$$

where ζ stands for the characteristic mesh size and u_{max} is the maximum value of the advection velocity along the z axis in the absence of any deposited particles. This implies that at most the particle can travel over a distance of one half a block sizes during the reference time. Previous studies [34, 37] have shown the relevance of this choice of the reference time for particle tracking.

The position of a moving particle is obtained by summing the old position vector $\mathbf{X}_{old}$ and the updated velocity multiplied by the reference time t_r:

$$\mathbf{X}_{new}=\mathbf{X}_{old}+ t_r\ \mathbf{V} \quad (6)$$

Table 1 Parameters used for simulations

Parameters	Values
Particle radius, a_p (m)	2×10^{-7}
Length of the capillary, L (m)	1.5×10^{-5}
Boltzmann constant, k (J/°K)	1.38×10^{-23}
Temperature, T (°K)	293.15
Dynamic viscosity, μ (Pa·s)	10^{-3}

During the particle tracking process, four situations may occur: (1) the particle leaves the domain without deposition (Figure 2a); (2) the center-to-center distance between the moving particle and any other particle already deposited is less than a predefined value, the transported particle will bounce back to the bulk flow, and the tracking process will continue (Figure 2b); (3) the distance between the particle center and the pore wall is less than a certain value (0.5 a_p), and the local surface wall is repulsive (positively charged), the transported particle will also bounce back to the bulk flow, and the tracking process will continue (Figure 2c); (4) the distance between the particle center to the pore wall is less than 0.5 a_p and the local surface wall is attractive (negatively charged), the particle will be deposited if enough free surface is available for deposition (Figure 2d). In that case, the meshes containing the deposited particle are considered as solid to take into account the finite particle volume, and the flow field is then recalculated and stored flow data are updated. As soon as the loop for one particle finishes, another particle is injected. The injection process is repeated until the particle deposition probability defined as the ratio of the number of deposited particles over the number of injected particles, reaches a minimum value of 2%. This approach was successfully used to describe colloids deposition in narrow pores of various shapes and is extended here to reconsider those phenomena in case of heterogeneous surfaces as presented in Figure 1 [34, 35, 37].

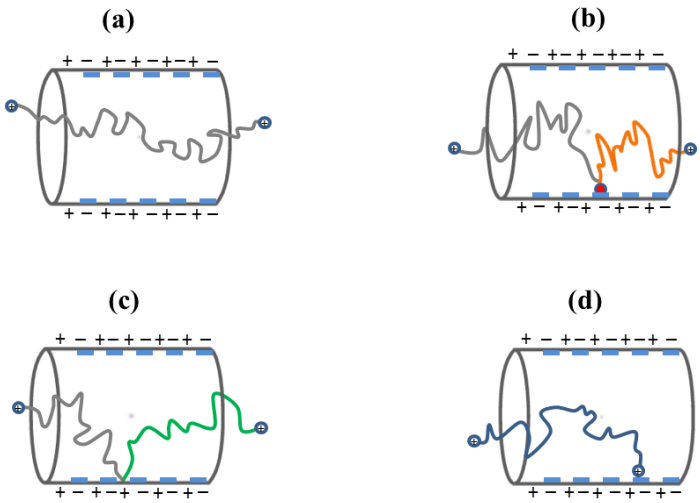

Figure 2 : Sketches of possible particle trajectories: (a) flowing through the capillary without deposition; (b) particle approaching a deposited particle (in grey line) and bouncing back to the bulk flow (in orange line); (c) particle approaching a repulsive zone and bouncing back to the bulk flow (in green line); (d) particle approaching an attractive zone and deposited when enough surface is available.

3. Results and discussion

3.1 crosswise strips case

Numerical simulations of particle transport and deposit have been performed in a capillary with a chemically heterogeneous surface patterned with crosswise strips. Here, for limiting lengthy numerical simulations, the analysis is restricted to one single value of favorable surface ratio, $\theta = 0.5$ and varying values of the strip frequency, λ.

3.1.1 Local deposition behavior

To assess tools and procedure capability, we first investigate the local structure of the deposit along the capillary. For that purpose, the geometry is divided into 10 slices along the z axis (the mean flow direction) and spatial distribution of deposited particles is calculated as the number of particles per unit area. It is worth noting that since gravity is ignored such a distribution is uniform in each cross section. As an illustration, on Figure 3a, we plotted the density profile along the capillary after injection of 2,000 particles at $Pe = 1.5\times10^{-3}$ taking $\theta = 0.5$ and $\lambda = 5$ for which the width of an adsorbing strip is four times the particle diameter. As it can be observed, the spatial distribution closely emulates the periodic nature of the heterogeneous pattern. Regarding the density trend in each adsorbing slice, peaks are seen to form at the leading and trailing edges as it was observed by others using Eulerian methods [32, 41]. Nazemifard and coworkers (2006) have proposed a phenomenological explanation of such phenomena that relies on coupled effects of hydrodynamic and colloidal interactions. When the particles are relatively far from the wall, they tend to accumulate over the unfavorable strips since they cannot get closer to the surface due to the energy barrier thereby locally depleting the immediate neighborhood of the wall. Consequently, with the presence of advection and diffusion, the particles can be transferred toward the nearest favorable strips, causing an enhanced density at the leading edges. Similarly, sharp concentration peaks are also observed at the trailing edges in the present work. It should be noted here that this phenomenon is

only dependent on the topology of the adsorbing/non-adsorbing zones, and should still hold for higher Pe, although it will be less spectacular since deposition density will be much lower (see hereafter). Another remarkable feature of these results are clearly seen when the actual density is compared to that obtained for homogeneous surfaces under the same conditions. It shows that deposition along the capillary is much more uniform than density corresponding to the homogeneous case. Similar behavior has also been reported by Chatterjee et al. [33] and Nazemifard et al. [32, 41] showing that in case of homogeneous surfaces most of particles will deposit within a very short distance from the inlet while heterogeneity make the deposit more uniform along the capillary. This means that particles tend to travel further along the heterogeneous capillary compared to homogeneous capillary. This is schematized in Figure 3c and Figure 3d that give 3D sectional views of deposit structure corresponding to each case.

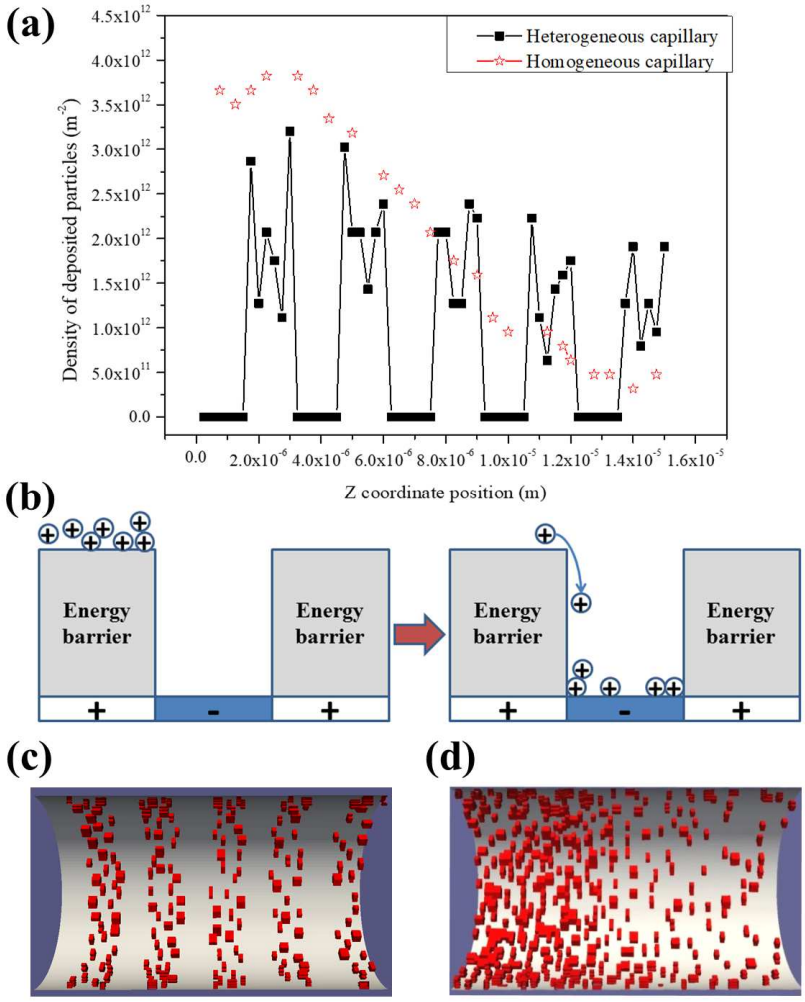

Figure 3 (a) Spatial density distribution of the deposited particles versus the z coordinate at N=2000, Pe = 1.5×10^{-3} for both heterogeneous ($\lambda = 5$ and $\theta = 0.5$) and homogeneous capillary; (b) schematic representation of particle behavior near the boundaries between the favorable and unfavorable strips (after Nazemifard et al. 2006). 3D sectional view of the heterogeneous (c) and homogeneous (d) capillary. The red objects represent the deposited particles; the flow occurs from left to right.

3.1.2 Deposition probability versus pitches frequency

Here we investigate the evolution of the deposition probability as a function of the number of injected particles (N) at $\theta = 0.5$ and a low Péclet number, Pe=1.5×10^{-3}. The particles deposition

probability is defined as the ratio of the number of deposited particles over the number of injected particles and is calculated over groups of 200 particles for each simulation run [3]. From one run to the other, λ was varied while keeping $w_a=w_{na}$. All the data are gathered in Figure 4 where the reference case of a homogeneous capillary is also shown for comparison purposes. For all λ values, we observe a behaviour that is usual in the diffusion-dominant regime with a plateau at the early stage of the injection process. As the number of injected particles increases, the deposition probability reaches a critical value; or a jamming probability; before it drops rather sharply to relatively low values, indicating that any newly injected particles will almost travel along the capillary without deposition [5]. This is similar to the well documented RSA process [42]. More importantly, deposition probability obviously increases with λ although θ is constant. This is because, large λ and consequently large number of favourable strips lead to an increase of the relative number of successful attempts of particles to adsorb and that is why adsorption kinetics and the jamming coverage increase significantly, at a fixed site density, when the ratio a_p/w_a increases [20]. As long as the strip width is greater than the mesh size, the behavior approaches that of a homogeneous adsorbing capillary for high λ values. The other interesting limit is for λ = 1 for which the first half of the capillary is non-adsorbing and the second half is adsorbing. In such a situation, there is a greater probability for a particle to be transported over the favorable section without deposition [33]. This demonstrates that for a given θ, the deposition probability is highly dependent on the distribution of the surface charge.

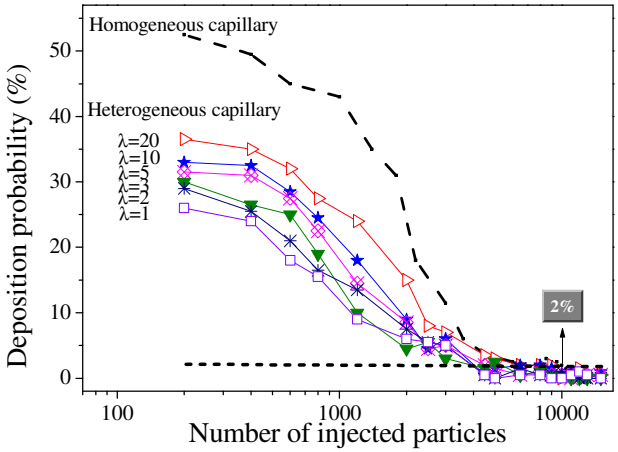

Figure 4 Variation of deposition probability versus the number of injected particles (N) for heterogeneous (with different λ) and homogeneous capillaries. ($Pe = 1.5\times10^{-3}$, θ = 0.5)

Moreover and as for a homogeneous adsorbing surface, the simulation results are represented in terms of the surface coverage (Γ) by dividing the total area of projection of deposited particles by the capillary surface. For the chemically heterogeneous surfaces, instead of the total capillary surface, only the adsorbing surface is used. Obtained results are commonly presented in dimensionless form Γ/Γ_{RSA} with Γ_{RSA} being the upper limit of surface coverage. Using the Random Sequential Adsorption (RSA) method, Γ_{RSA} equals 0.546 for non-interacting hard spheres adsorbing on a homogeneous flat surface under diffusion regime [42]. On Figure 5, the variation of Γ/Γ_{RSA} versus the number of injected particles is plotted, where the dependence on λ for θ = 0.5 under diffusion-dominant regime can be examined. It should be noted that as long as λ is low, adsorption efficiency is small and the asymptotic value of Γ/Γ_{RSA} is significantly below unity due to low deposition probability. For high λ, however, the adsorbing efficiency is clearly promoted by the thinness of adsorbing slices and Γ is significantly higher than Γ_{RSA} as a consequence of the fact that the projection of adsorbed particles often go beyond the border of adsorbing slices.

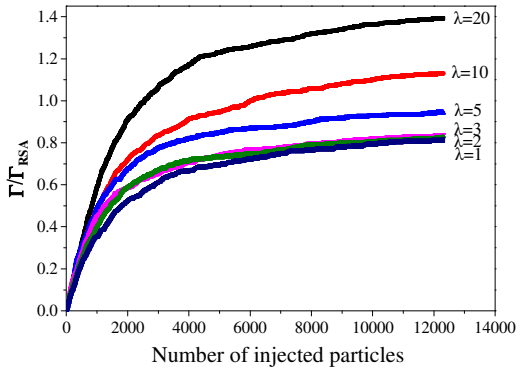

Figure 5 Variation of the dimensionless surface coverage versus N for a heterogeneous capillary with different λ (Pe=1.5×10^{-3}, θ=0.5).

3.1.3 Influence of the Péclet number

To go further, the dependence of Γ/Γ_{RSA} on Pe was considered in order to investigate the influence of the flow strength and its induced changes on the structure of the deposit. For that purpose, seven simulation runs were carried out over 6 decades with Pe ranging from 1.5×10^{-3} to 1.5×10^{3}, while keeping both θ and λ constant (θ=0.5 and λ=5). The raw data corresponding to each Pe value was first plotted in terms of Γ/Γ_{RSA} versus the number of injected particles. The latter was increased until the deposition probability reached 2%. Finally, the asymptotic values of Γ/Γ_{RSA} were plotted against Pe. Obtained results are displayed on Figure 6 showing the existence of two distinct regimes: a diffusion-dominant regime for low Péclet numbers and a advection-dominant regime at high Péclet numbers that are connected through a transition regime. In the diffusion-dominant regime, the surface coverage is almost independent of Pe while in the advection-dominant one, the surface coverage is a decreasing function of Pe. At low Pe, deposition is a RSA-like Process and features a plateau while when particles transport is mainly governed by advection, the hydrodynamic shadowing effect comes into play. This well documented phenomenon [43, 44] is named so since, in this regime, there is an exclusion area behind already adsorbed particles that is prohibited for newly injected ones. By increasing Pe, such a surface is consequently increased resulting in a decrease of the surface coverage [5, 45]. This behavior is in all respects similar to the case of a homogeneous capillary as one could expect. It is to be noted that the value of Γ_{RSA} used for scaling the data in Figure 6 is dependent on λ (asymptotic values in Figure 5) and is of 0.546 for homogeneous case. This Péclet dependent surface coverage was evidenced in column experiments when latex particle suspensions are let to flow at increasing velocity in adsorbing sandpack porous media [9]. Although obtained surface coverage data were plotted as a function of fluid velocity rather than Péclet number, their results are very similar to those shown on figure 6. Similar results were also found in case of experiments performed on columns packed with silicone carbide [45]. It was also numerically evidenced by studying colloid deposition in adsorbing pores of various shapes [34, 37]. Marijn and co-workers [46] have investigated latex particles deposition on a flat adsorbing surface under unidirectional laminar flow conditions. They showed experimentally that, in advection dominant regime, the characteristic length of the exclusion area along the flow direction should increase with Pe as Pe^{n}, with n =0.87. However other investigations based on theoretical considerations predict that the Sherwood number; Sh, that represents the non-dimensional flux of particles toward collecting surface should scale as Pe$^{1/3}$ [32, 41, 47]. Because the density of adsorbing particles and hence the surface coverage is proportional to the colliding flux multiplied by the collection efficiency, η, and as η is predicted to depend on Pe as Pe$^{-2/3}$ [48], Γ is expected to decrease as Pe$^{-1/3}$ in the advection

dominant regime. This power law is displayed on figure 6 showing a reasonable agreement with our results. It must be noted, however, that in previous works on homogeneous adsorbing surfaces [34, 37, 45] a closer fit was found with this power law.

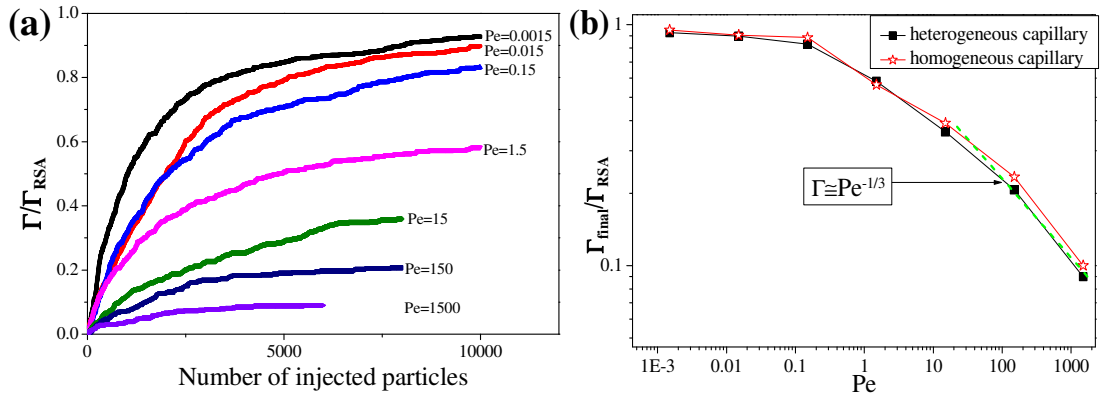

Figure 6 Variation of dimensionless surface coverage Γ/Γ_{RSA} for the chemically heterogeneous capillary, $\lambda = 5$ and $\theta = 0.5$ (a) Γ/Γ_{RSA} versus N at different Pe; (b) $\Gamma_{final}/\Gamma_{RSA}$ as a function of Pe.

3.2 Chess board patterned case

In this section, the focus is laid upon heterogeneity consisting of chess board patterns. Moreover to compare deposition in the present case with the former one, the test case is restricted to one surface ratio value, $\theta = 0.5$, and to diffusion-dominant regime where the deposit probability is significant.

3.2.1 Surface coverage

For the case of chess board patterned capillaries, as for alternating adsorbing non-adsorbing strips, first square patches of equal size of 3 μm were considered, so that $\lambda = 5$ along any generating line and an adsorbing surface fraction of $\theta = 0.5$ (see Figure 1). The runs were performed in the diffusive regime taking $Pe = 1.5\times10^{-3}$ and particles deposition was followed by varying the number of injected particles until adsorption was over. A sectional view of the deposit is shown on figure 7a for both kinds of spatial distribution of chemical heterogeneity. However, since it is difficult to draw any conclusions from this view of deposit, again the variation of Γ/Γ_{RSA} as a function of the number of injected particles, N, is displayed on figure 7b. Then we may note that at low N values, the surface coverage is a linear function of N for both heterogeneity patterns. Since such a situation corresponds to clean bed conditions, the effective collection efficiency; η_{eff}; or the slope of these curves, is the same in both cases suggesting that this property is insensitive to the pattern form and only depends on θ and λ. For large N however, it could be seen that Γ/Γ_{RSA} corresponding to the chess board pattern is higher than in case of transverse strips. Indeed, as we emphasized in section 3.1, the average density of deposited particles at the leading and trailing edges of a favorable zone is often greater than its mean value over the whole zone. Thereby the observed results are direct consequences of higher deposition probability and the increase of total contour length of the heterogeneity area when a chess board pattern is adopted. Pham et al. [49] have reported similar behavior by numerically investigating nano-particles deposition in packed beds with four different patterns of surface charge heterogeneity and the same fraction of favorable surface. In their work spherical collectors that are favorable for nano-particles attachment are placed at different locations.

They show that when heterogeneity is randomly or uniformly distributed, nano-particles capture is more efficient compared to the case of transverse strip pattern. Indeed, for the chess board patterned capillary or more generally a random mixture pattern, the particles have more time and higher opportunity to move towards and collide with the favorable surfaces as they propagate through the domain.

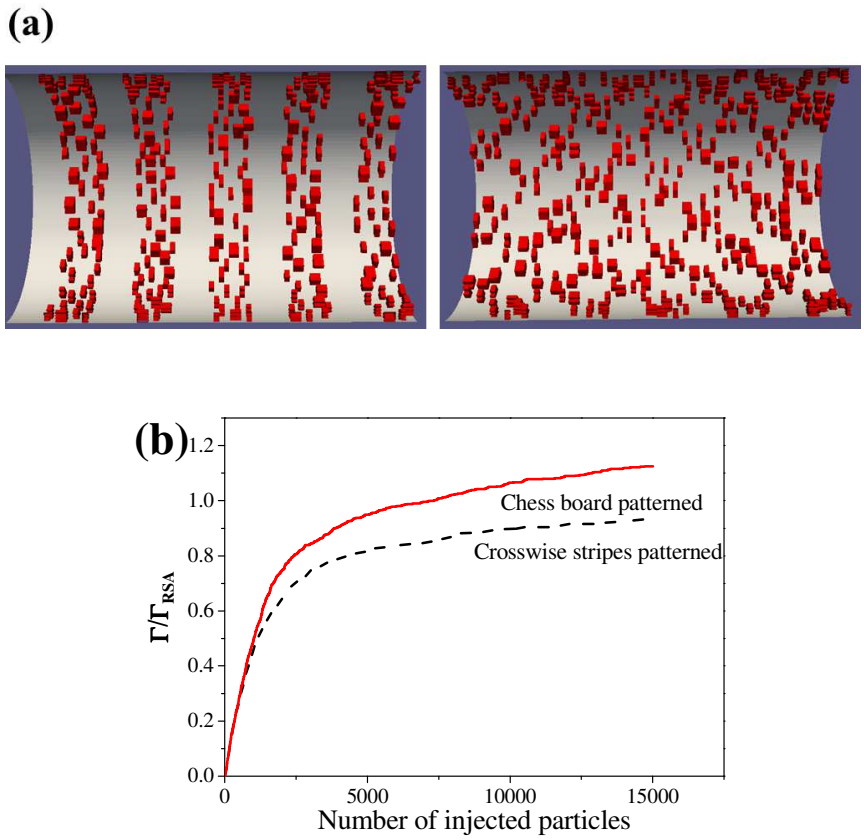

Figure 7 (a) 3D sectional view (left: crosswise strips patterned), (right: chess board patterned) of the heterogeneous capillary with deposited particles; (b) variation of dimensionless surface coverage Γ/Γ_{RSA} versus the number of injected particles, N, for crosswise strips patterned and chess board patterned capillaries. For both cases, $\theta = 0.5$, pitch length = 3 μm and $Pe = 1.5\times10^{-3}$.

3.2.2 Effect of the favorable surface ratio

In order to investigate the influence of a favorable surface ratio, θ, on particles deposition, nine simulation runs were carried out at the same $Pe = 1.5\times10^{-3}$ for θ ranging from 0.2 to 1. In these simulations, the pattern was unchanged keeping $\lambda = 5$ but the size of adsorbing patches was modified to give different values of θ. Again, the obtained results are first presented in terms of the number of deposited particles versus the number of incoming particles and all the data are gathered in figure 8. For a chemically heterogeneous porous medium consisting in a random distribution of favorable and unfavorable zones, the deposition efficiency also named the effective efficiency $\eta_{effective}$ is generally given simply as a weighted average of favorable and unfavorable deposition efficiencies:

$$\eta_{effective} = \theta\eta_f + (1-\theta)\eta_u \qquad (9)$$

where η_f and η_u stand respectively for favorable and unfavorable deposition efficiencies. Since the particle can only adsorb if the projection of its center lies within the favorable zone, and no particles can deposit on an unfavorable one ($\eta_u = 0$), equation (9) simplifies to:

$$\frac{\eta_{\text{effective}}}{\eta_{\text{f}}} = \theta \tag{10}$$

For comparison, the value of $\eta_{effective}/\eta_f$ predicted Eq. 10 (the dashed line), and those obtained from our simulations (the solid squares) are plotted in Figure 8c. $\eta_{effective}$ is the slope of 8(b) at the early stages of deposition process corresponding to clean bed conditions for each θ value and η_f is the deposition efficiency for a completely favorable surface. Eq. 10 provides a remarkably accurate prediction of the deposition efficiency for surfaces with macroscopic charge heterogeneity, even when the dimension of the heterogeneous zones is comparable to the particle dimensions.

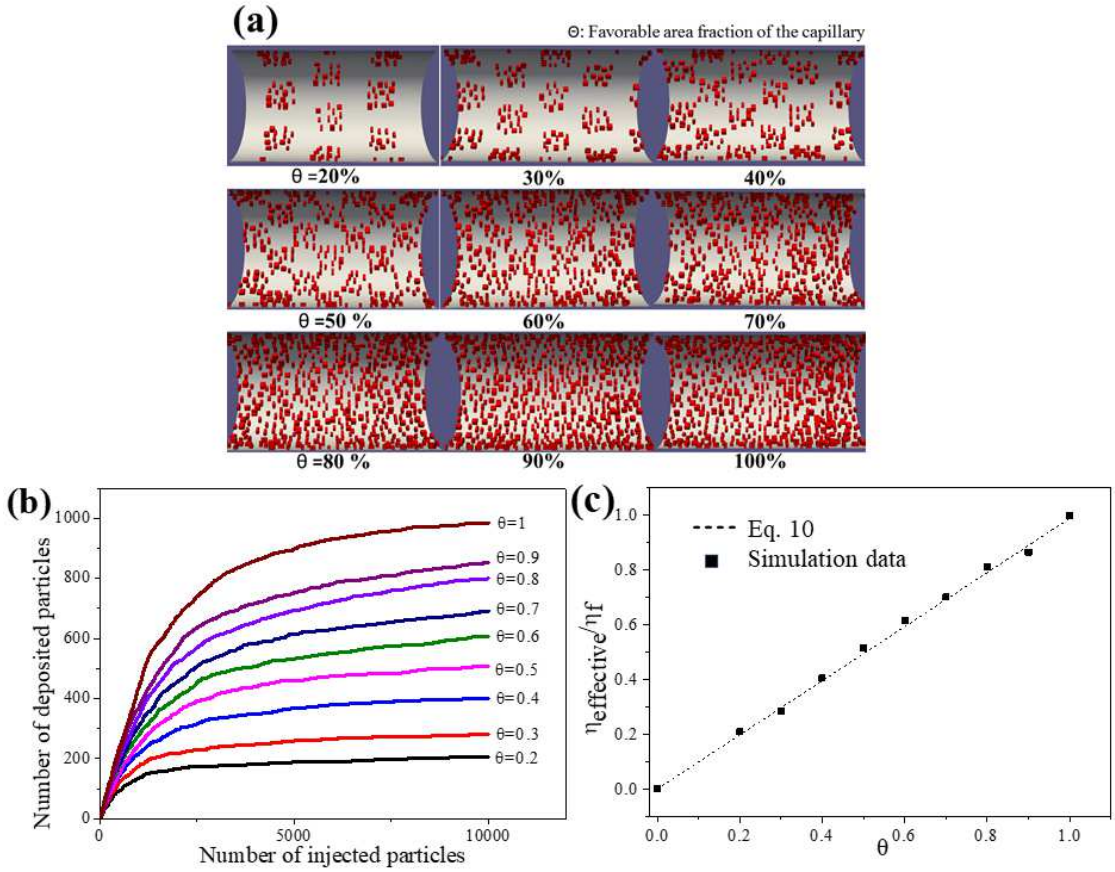

Figure 8 (a) 3D sectional view of the heterogeneous capillary with deposited particles, λ = 5, Pe = 1.5×10^{-3}, θ is ranging from 0.2 to 1; (b) variation of the number of deposited particles versus the number of injected particles (N) with different θ; (c) the dependence of the effective collector efficiency ($\eta_{effective}/\eta_f$) on θ (λ = 5, Pe = 1.5×10^{-3}).

4. Conclusions

In this work, the proposed 3D-PTPO code is shown to be a useful and flexible tool for the microscale simulation of colloidal particle transport and deposition in a 3D chemically heterogeneous capillary. The main conclusions that can be drawn are as follows:

(i) The coupled effect of the charge heterogeneity and the three-dimensional velocity field can bring out a complex concentration distribution of deposited particles on the wall, leading to a higher density of deposited particles at the leading and trailing edges of each favorable strip, and the deposition is more uniform along the patterned capillary compared to the homogeneous one.

(ii) The deposition probability is in line with the frequency of the pitches. Under the same favorable surface ratio, θ, a smaller pitch length will result in a higher deposition probability and accordingly a higher dimensionless surface coverage. Moreover, for the diffusion-dominant regime at low Pe, the surface coverage is close to the Γ_{RSA} and features a relatively stable plateau. For the advection-dominant regime at high Pe, the declining trend of Γ/Γ_{RSA} versus Pe is in good agreement with the derived power law dependence of surface coverage versus Pe for the considered ratios a_p/w_a.

(iii) The deposition efficiency increases linearly with the favorable area fraction. Although the simulations performed are not exhaustive and have been limited to special choices of Péclet number and/or favorable surface ratio, this study provides insight in designing artificially heterogeneous porous media for particle capture in various engineering and biomedical applications. Furthermore, the model can be further improved by incorporating other heterogeneous patterns and more importantly by decreasing the capillary size to particle size.

Declarations of interest

None.

Acknowledgement

This work was supported in part by the China Scholarship Council (CSC) under the Grant CSC N° 201506260062, and the Shanghai Pujiang Program (No. 2019PJD016).

References:

[1] T. Tosco, J. Bosch, R.U. Meckenstock, R. Sethi, Transport of ferrihydrite nanoparticles in saturated porous media: role of ionic strength and flow rate, Environ. Sci. Technol., 46 (2012) 4008-4015.

[2] I.S. Ngene, R.G. Lammertink, M. Wessling, W. van der Meer, A microfluidic membrane chip for in situ fouling characterization, J. Membr. Sci., 346 (2010) 202-207.

[3] B. Asgharian, O. Price, W. Hofmann, Prediction of particle deposition in the human lung using realistic models of lung ventilation, J. Aerosol Sci, 37 (2006) 1209-1221.

[4] S. Bensaid, D.L. Marchisio, D. Fino, Numerical simulation of soot filtration and combustion within diesel particulate filters, Chem. Eng. Sci., 65 (2010) 357-363.

[5] K.-M. Yao, M.T. Habibian, C.R. O'Melia, Water and waste water filtration. Concepts and applications, Environ. Sci. Technol., 5 (1971) 1105-1112.

[6] M. Elimelech, C.R. O'Melia, Kinetics of deposition of colloidal particles in porous media, Environ. Sci. Technol., 24 (1990) 1528-1536.

[7] M. Elimelech, C.R. O'Melia, Effect of particle size on collision efficiency in the deposition of Brownian particles with electrostatic energy barriers, langmuir, 6 (1990) 1153-1163.

[8] J.N. Ryan, M. Elimelech, Colloid mobilization and transport in groundwater, Colloids Surf. Physicochem. Eng. Aspects, 107 (1996) 1-56.

[9] C.-H. Ko, S. Bhattacharjee, M. Elimelech, Coupled influence of colloidal and hydrodynamic interactions on the RSA dynamic blocking function for particle deposition onto packed spherical collectors, J. Colloid Interface Sci., 229 (2000) 554-567.

[10] N. Tufenkji, J.A. Redman, M. Elimelech, Interpreting deposition patterns of microbial particles in laboratory-scale column experiments, Environ. Sci. Technol., 37 (2003) 616-623.

[11] X. Li, W.P. Johnson, Nonmonotonic variations in deposition rate coefficients of microspheres in porous media under unfavorable deposition conditions, Environ. Sci. Technol., 39 (2005) 1658-1665.

[12] Z. Adamczyk, B. Siwek, M. Zembala, Reversible and irreversible adsorption of particles on homogeneous surfaces, Colloids and surfaces, 62 (1992) 119-130.

[13] Z. Adamczyk, T. Dabros, J. Czarnecki, T.G. Van De Ven, Particle transfer to solid surfaces, Adv. Colloid Interface Sci., 19 (1983) 183-252.
[14] R. Rajagopalan, C. Tien, Trajectory analysis of deep‐bed filtration with the sphere‐in‐cell porous media model, AlChE J., 22 (1976) 523-533.
[15] M. Elimelech, Particle deposition on ideal collectors from dilute flowing suspensions: Mathematical formulation, numerical solution, and simulations, Separations Technology, 4 (1994) 186-212.
[16] M. Elimelech, Kinetics of capture of colloidal particles in packed beds under attractive double layer interactions, J. Colloid Interface Sci., 146 (1991) 337-352.
[17] I.L. Molnar, W.P. Johnson, J.I. Gerhard, C.S. Willson, D.M. O'Carroll, Predicting colloid transport through saturated porous media: A critical review, Water Resour. Res., 51 (2015) 6804-6845.
[18] J.P. Loveland, S. Bhattacharjee, J.N. Ryan, M. Elimelech, Colloid transport in a geochemically heterogeneous porous medium: aquifer tank experiment and modeling, J. Contam. Hydrol., 65 (2003) 161-182.
[19] J.Y. Chen, C.-H. Ko, S. Bhattacharjee, M. Elimelech, Role of spatial distribution of porous medium surface charge heterogeneity in colloid transport, Colloids Surf. Physicochem. Eng. Aspects, 191 (2001) 3-15.
[20] Z. Adamczyk, P. Weroński, E. Musiał, Irreversible adsorption of hard spheres at random site (heterogeneous) surfaces, The journal of chemical physics, 116 (2002) 4665-4672.
[21] Z. Adamczyk, B. Siwek, K. Jaszczółt, P. Weroński, Deposition of latex particles at heterogeneous surfaces, Colloids Surf. Physicochem. Eng. Aspects, 249 (2004) 95-98.
[22] Z. Adamczyk, K. Jaszczółt, B. Siwek, Irreversible adsorption of colloid particles on heterogeneous surfaces, Appl. Surf. Sci., 252 (2005) 723-729.
[23] H. Unni, C. Yang, Brownian dynamics simulation and experimental study of colloidal particle deposition in a microchannel flow, J. Colloid Interface Sci., 291 (2005) 28-36.
[24] Y.-I. Chang, S.-C. Chen, E. Lee, Prediction of Brownian particle deposition in porous media using the constricted tube model, J. Colloid Interface Sci., 266 (2003) 48-59.
[25] K. Fukagata, S. Zahrai, F.H. Bark, Dynamics of Brownian particles in a turbulent channel flow, Heat Mass Transfer., 40 (2004) 715-726.
[26] J.A. Kemps, S. Bhattacharjee, Particle tracking model for colloid transport near planar surfaces covered with spherical asperities, Langmuir, 25 (2009) 6887-6897.
[27] M. Mahdavi, M. Sharifpur, J.P. Meyer, Natural convection study of Brownian nano-size particles inside a water-filled cavity by LAGRANGIAN-Eulerian Tracking Approach, (2016).
[28] M. Mahdavimanesh, A. Noghrehabadi, M. Behbahaninejad, G. Ahmadi, M. Dehghanian, Lagrangian particle tracking: model development, Life Science Journal, 10 (2013) 34-41.
[29] F. Coutelieris, M. Kainourgiakis, A. Stubos, Low Peclet mass transport in assemblages of spherical particles for two different adsorption mechanisms, J. Colloid Interface Sci., 264 (2003) 20-29.
[30] J.A. Kemps, S. Bhattacharjee, Interactions between a solid spherical particle and a chemically heterogeneous planar substrate, Langmuir, 21 (2005) 11710-11721.
[31] R. Chatterjee, S.K. Mitra, S. Bhattacharjee, Particle deposition onto janus and patchy spherical collectors, Langmuir, 27 (2011) 8787-8797.
[32] N. Nazemifard, J.H. Masliyah, S. Bhattacharjee, Particle deposition onto charge heterogeneous surfaces: convection− diffusion− migration model, Langmuir, 22 (2006) 9879-9893.
[33] R. Chatterjee, S. Bhattacharjee, S.K. Mitra, Particle transport in patterned cylindrical microchannels, Microfluid. Nanofluid., 12 (2012) 41-51.

[34] Y. Li, A. Ahmadi, A. Omari, H. Pu, Three-dimensional microscale simulation of colloidal particle transport and deposition in model porous media with converging/diverging geometries, Colloids Surf. Physicochem. Eng. Aspects, 544 (2018) 179-186.
[35] Y. Li, O. Sarishvili, A. Omari, A. Ahmadi, H. Pu, Colloidal Particle Deposition in Porous Media Under Flow: A Numerical Approach, International Journal of Modeling and Optimization, International Journal of Modeling and Optimization vol. 7, no. 1, (2017) pp. 43-47.
[36] J.D.C. Díaz, P.G. Nieto, D. Castro-Fresno, P.M. Rodríguez, Steady state numerical simulation of the particle collection efficiency of a new urban sustainable gravity settler using design of experiments by FVM, Applied mathematics and computation, 217 (2011) 8166-8178.
[37] P. Lopez, A. Omari, G. Chauveteau, Simulation of surface deposition of colloidal spheres under flow, Colloids Surf. Physicochem. Eng. Aspects, 240 (2004) 1-8.
[38] F. Wirner, Flow and transport of colloidal suspensions in porous media, (2015).
[39] U. Dieter, Pseudo-random numbers. The exact distribution of pairs, Mathematics of computation, 25 (1971) 855-883.
[40] A. Djehiche, M. Gafsi, V. Canseco, A. Omari, H. Bertin, Effet de la force ionique et hydrodynamique sur le dépôt de particules colloïdales dans un milieu poreux consolidé, The Canadian journal of chemical engineering, 93 (2015) 781-787.
[41] N. Nazemifard, J.H. Masliyah, S. Bhattacharjee, Particle deposition onto micropatterned charge heterogeneous substrates: Trajectory analysis, J. Colloid Interface Sci., 293 (2006) 1-15.
[42] J. Talbot, G. Tarjus, P. Van Tassel, P. Viot, From car parking to protein adsorption: an overview of sequential adsorption processes, Colloids Surf. Physicochem. Eng. Aspects, 165 (2000) 287-324.
[43] J. Toth, Adsorption Theory, Modeling and Analysis, New York: Marcel Dekker (2002).
[44] S. Sasidharan, S. Torkzaban, S.A. Bradford, P.J. Dillon, P.G. Cook, Coupled effects of hydrodynamics and solution chemistry on long-term nanoparticle transport and deposition in saturated porous media, Colloid and Surfaces A: Physicochem. Eng. Aspects 457 (2014), 169-179.
[45] J. Veerapen, B. Nicot, G. Chauveteau, In-depth permeability damage by particle deposition at high flow rates, SPE European Formation Damage Conference, Society of Petroleum Engineers, 2001.
[46] M.T. van Loenhout, E.S. Kooij, H. Wormeester, B. Poelsema, Hydrodynamic flow induced anisotropy in colloid adsorption, Colloids Surf. Physicochem. Eng. Aspects, 342 (2009) 46-52.
[47] F. Coutelieris, M. Kainourgiakis, A. Stubos, The effect of Peclet on the Sherwood number in high porosity granular media, Stud. Surf. Sci. Catal., Elsevier2002, pp. 753-760.
[48] W. Russel, D. Saville, W. Schowalter, Colloidal Dispersions Cambridge Univ, Press, 1989.
[49] N.H. Pham, D.V. Papavassiliou, Effect of spatial distribution of porous matrix surface charge heterogeneity on nanoparticle attachment in a packed bed, Phys. Fluids, 29 (2017) 082007.

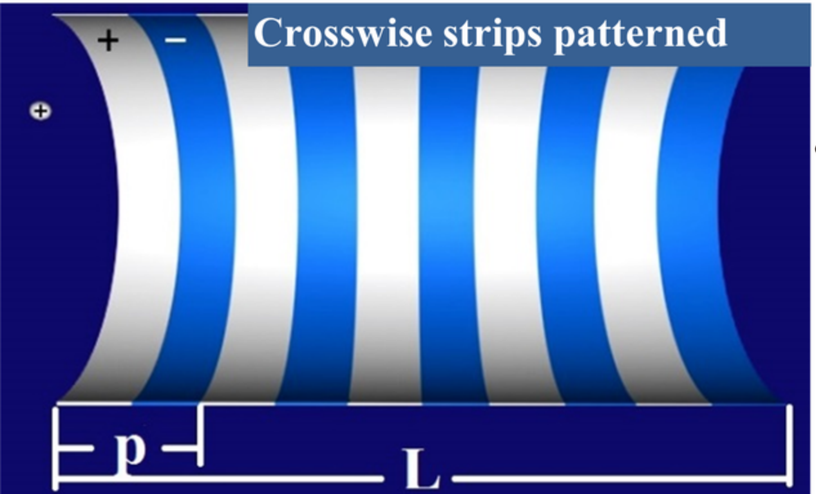
Crosswise strips patterned
+
−
p
L

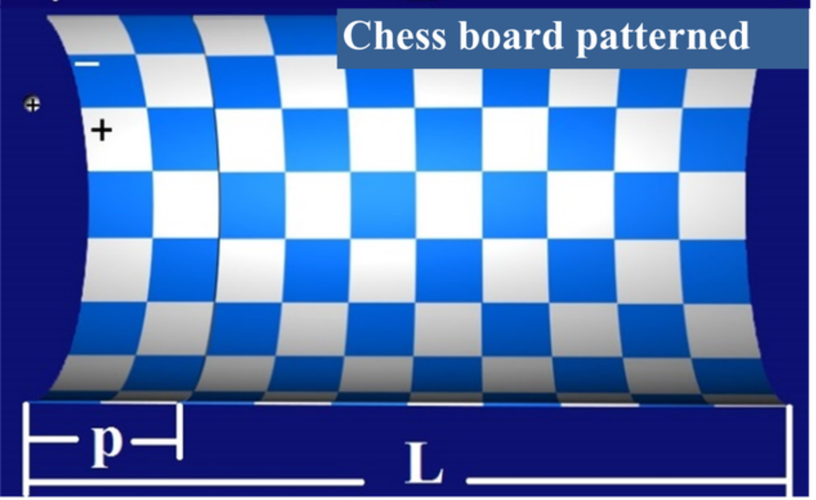
Chess board patterned
−
+
p
L

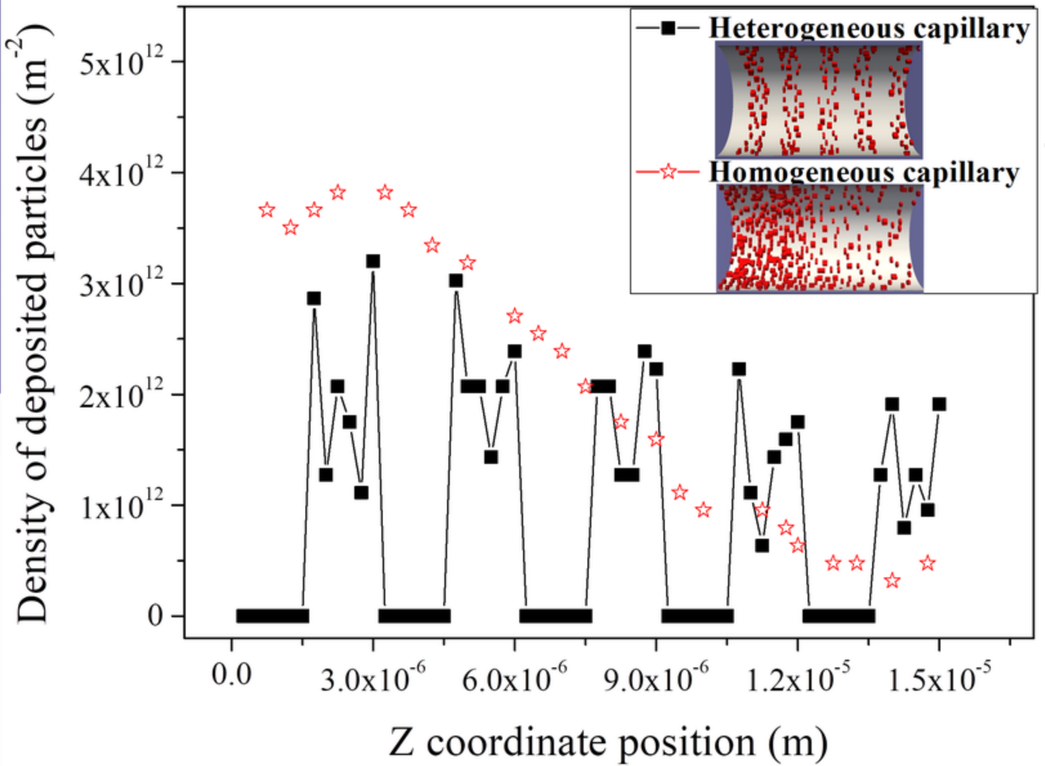
Heterogeneous capillary
Homogeneous capillary
Density of deposited particles (m-2)
5x10^12
4x10^12
3x10^12
2x10^12
1x10^12
0
0.0
3.0x10^-6
6.0x10^-6
9.0x10^-6
1.2x10^-5
1.5x10^-5
Z coordinate position (m)

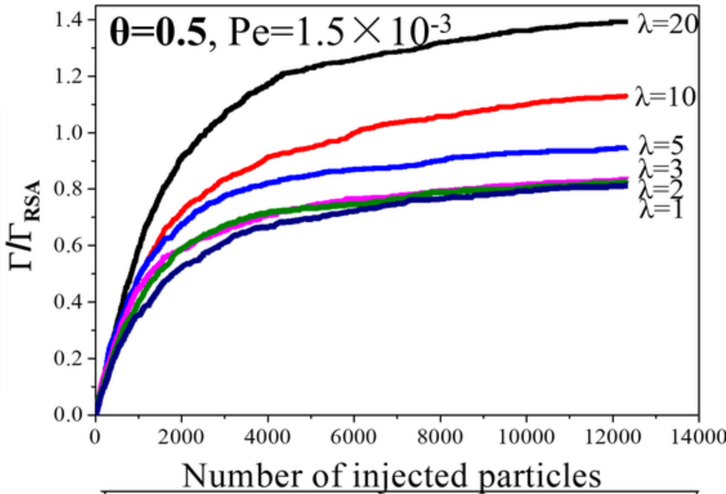
θ=0.5, Pe=1.5×10-3
λ=20
λ=10
λ=5
λ=3
λ=2
λ=1
Γ/ΓRSA
0.0
0.2
0.4
0.6
0.8
1.0
1.2
1.4
0
2000
4000
6000
8000
10000
12000
14000
Number of injected particles

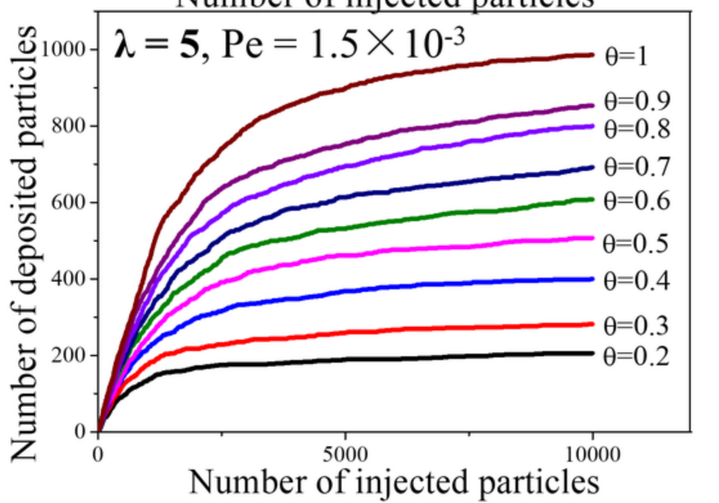
λ = 5, Pe = 1.5×10-3
θ=1
θ=0.9
θ=0.8
θ=0.7
θ=0.6
θ=0.5
θ=0.4
θ=0.3
θ=0.2
Number of deposited particles
0
200
400
600
800
1000
0
5000
10000
Number of injected particles